

Characterization of an Earthquake Sequence Triggered by Hydraulic Fracturing in Harrison County, Ohio

by Paul A. Friberg, Glenda M. Besana-Ostman, and Ilya Dricker

Online Material: Tables of hypoinverse earthquake locations and velocity models.

INTRODUCTION

To extract oil and gas in tight shale formations, hydraulic fracturing is used to stimulate fracture growth and increase permeability. Typically, low (-3.0 to $0.0 M_w$) magnitude earthquakes are produced during hydraulic fracturing (Maxwell *et al.*, 2002, 2009). In a few cases, however, hydraulic fracturing has been linked to widely observed larger, so-called positive magnitude, earthquakes. Examples include earthquakes felt by the general population in such areas as Blackpool, England, $M_L 2.3$ (de Pater and Baisch, 2011), Horn River Basin, Canada, $M_L 3.8$ (British Columbia Oil and Gas Commission [BCOGC], 2012), and Oklahoma $M_L 2.9$ (Holland, 2011, 2013) and more recently in Ohio (Skoumal, 2014). In this paper, we show the first evidence of positive magnitude earthquakes on a previously unmapped fault in Harrison County, Ohio, that can be related to a hydraulic fracture operation.

REGIONALLY LOCATED EVENTS

A series of six earthquakes were located by the Array Network Facility regional seismic network using the Incorporated Research Institutions for Seismology (IRIS) EarthScope Transportable Array (TA) stations in Ohio on 2 October 2013. These earthquakes were located south of Clendenning Lake in Harrison County near the town of Uhrichsville, Ohio, and included two $M_w 2.0$ events. This series of earthquakes was followed by four more events with $M_w 1.7$ – 2.2 from 3 to 19 October. There were no felt reports for any of these earthquakes. Upon inspection of the OhioSeis seismic network catalog (Hansen and Ruff, 2003) and other available historical catalogs in the region (Stover and Coffman, 1993), this series of earthquakes is the first known seismic occurrence in the region.

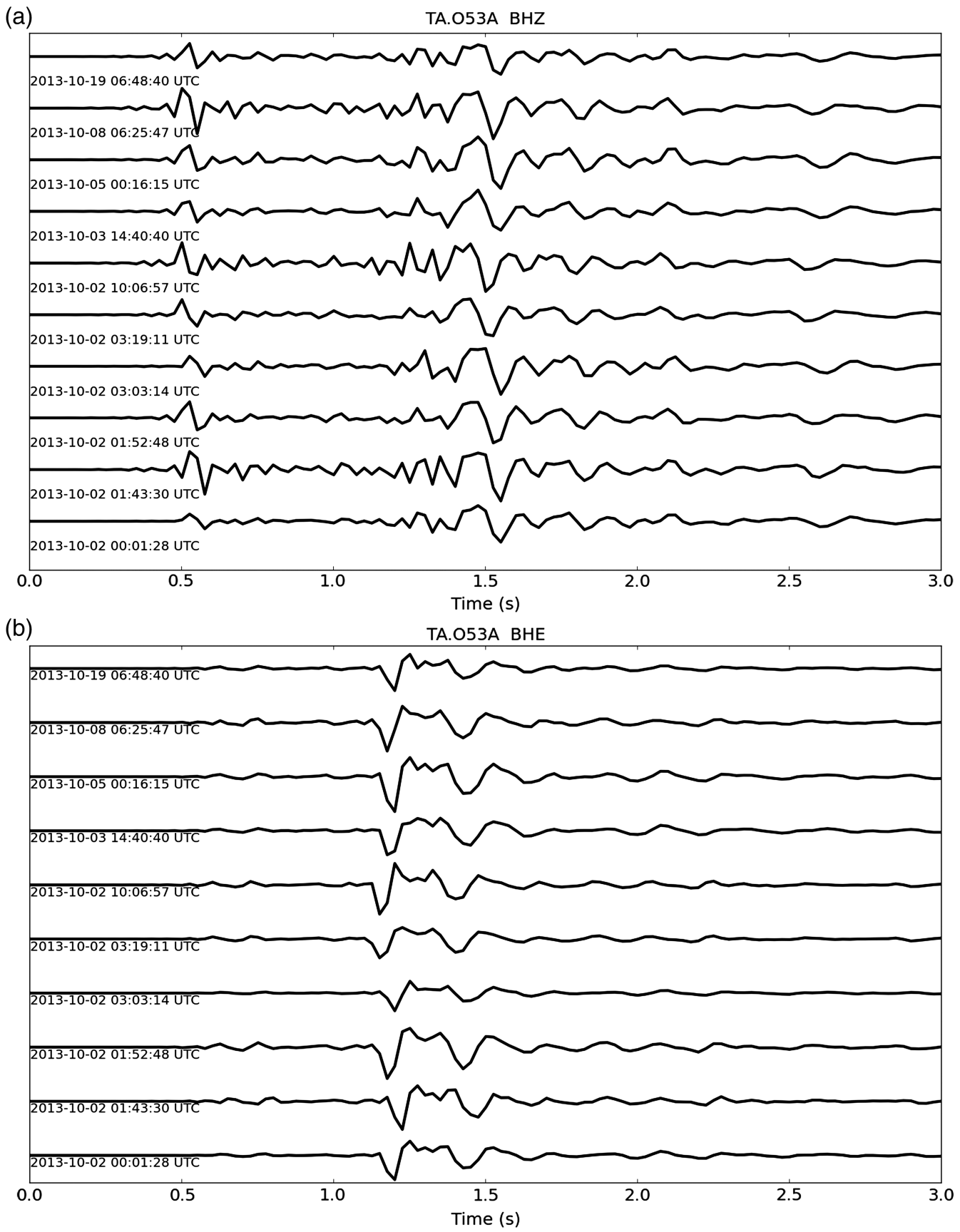
The closest station to the earthquakes was the IRIS EarthScope TA O53A station located within 2–3 km of the earthquakes based on S – P times of 0.66 ± 0.02 s for all 10 earthquakes (Table S1, available in the electronic supple-

ment to this article). Notably, the waveforms at TA O53A of each of the earthquakes were remarkably similar (Fig. 1) suggesting that all seismic events were from the same source.

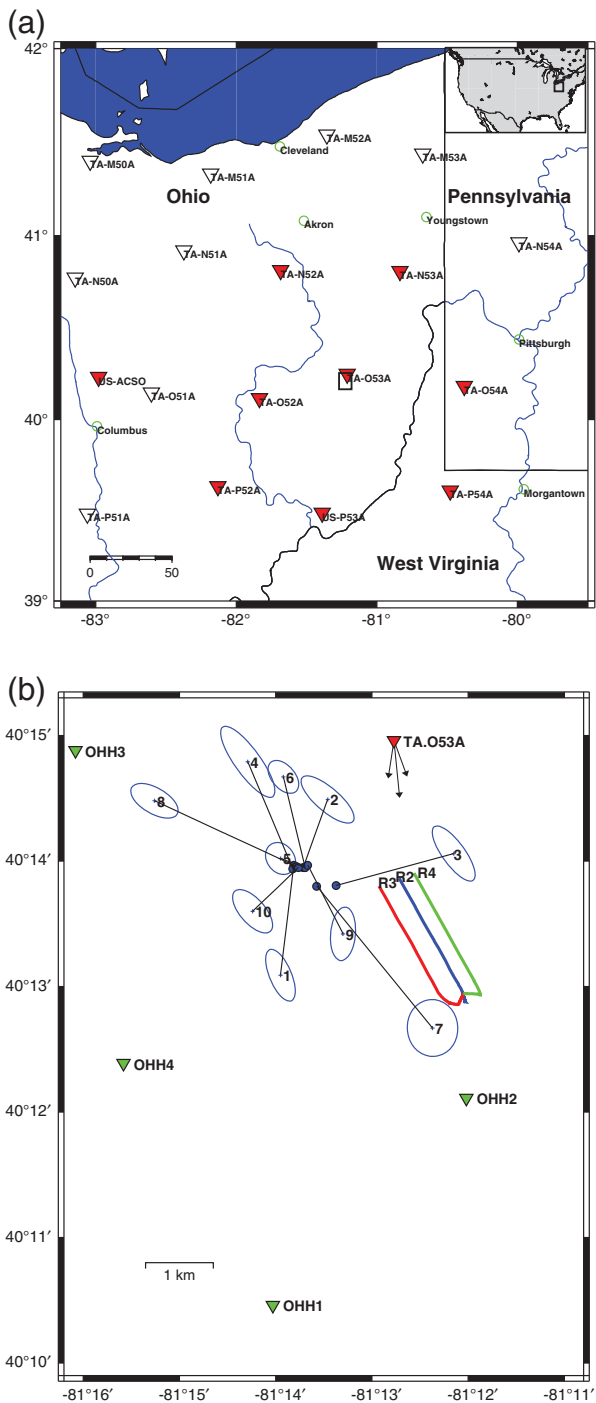
Initial locations of the earthquakes were calculated by manually picking P and S arrivals using SeisAn software (Havskov and Ottemöller, 1999) and via HYPOCENTER location algorithm (Lienert *et al.*, 1986; Lienert and Havskov, 1995). We used a regional 1D velocity model, herein called “NE Ohio” velocity model (Hansen and Ruff, 2003; Kim, 2013) with a V_p/V_s of 1.73 (Table S2). The initial locations of the earthquakes were widely distributed laterally and vertically and showed no pronounced clustering. Moment magnitudes for each of the earthquakes were determined using SeisAn’s spectral long-period displacement fitting algorithm (Ottemöller and Havskov, 2003) using the average M_w of the five closest TA stations.

All 10 earthquakes were then relocated using the NE Ohio velocity model and HYPOINVERSE (Klein, 2007) to obtain an improved uncertainty ellipsoid and improved precision in starting location (Fig. 2b). The earthquakes had an average root mean square (rms) of 0.062 s, average vertical uncertainty of ± 732 m, and average horizontal uncertainty of ± 432 m. Using manual phase picks to relocate the earthquakes with the double-difference algorithm HypoDD (Waldhauser and Ellsworth, 2000; Waldhauser, 2001) showed no pronounced structure responsible for the sequence. Employing waveform cross-correlation techniques around the phase arrivals (Schaff, 2008; Schaff and Waldhauser, 2010) along with the manual phase picks, however, helped to better constrain the relative locations (Fig. 2b). After HypoDD relocations on the combined data, the seismicity defined roughly a linear pattern oriented east–west as the possible source of the earthquakes with depth ranges of 3.8–4.0 km. The HypoDD relative uncertainty derived from the singular value decomposition (SVD) option was ± 84 m longitudinal, ± 107 m latitudinal, and ± 115 m vertical. Unfortunately, first-motion focal mechanisms could not be obtained for any of the earthquakes due to noisy data at more distant stations and inadequate station distribution.

To better constrain the absolute location of the regional cluster, we performed back-azimuth analysis on three-component data of TA O53A station using the method of



▲ **Figure 1.** Normalized *P*-wave aligned waveforms from 053A's (a) vertical component, BHZ, and (b) one horizontal component, BHE, channels for 10 earthquakes located using Transportable Array (TA) stations.



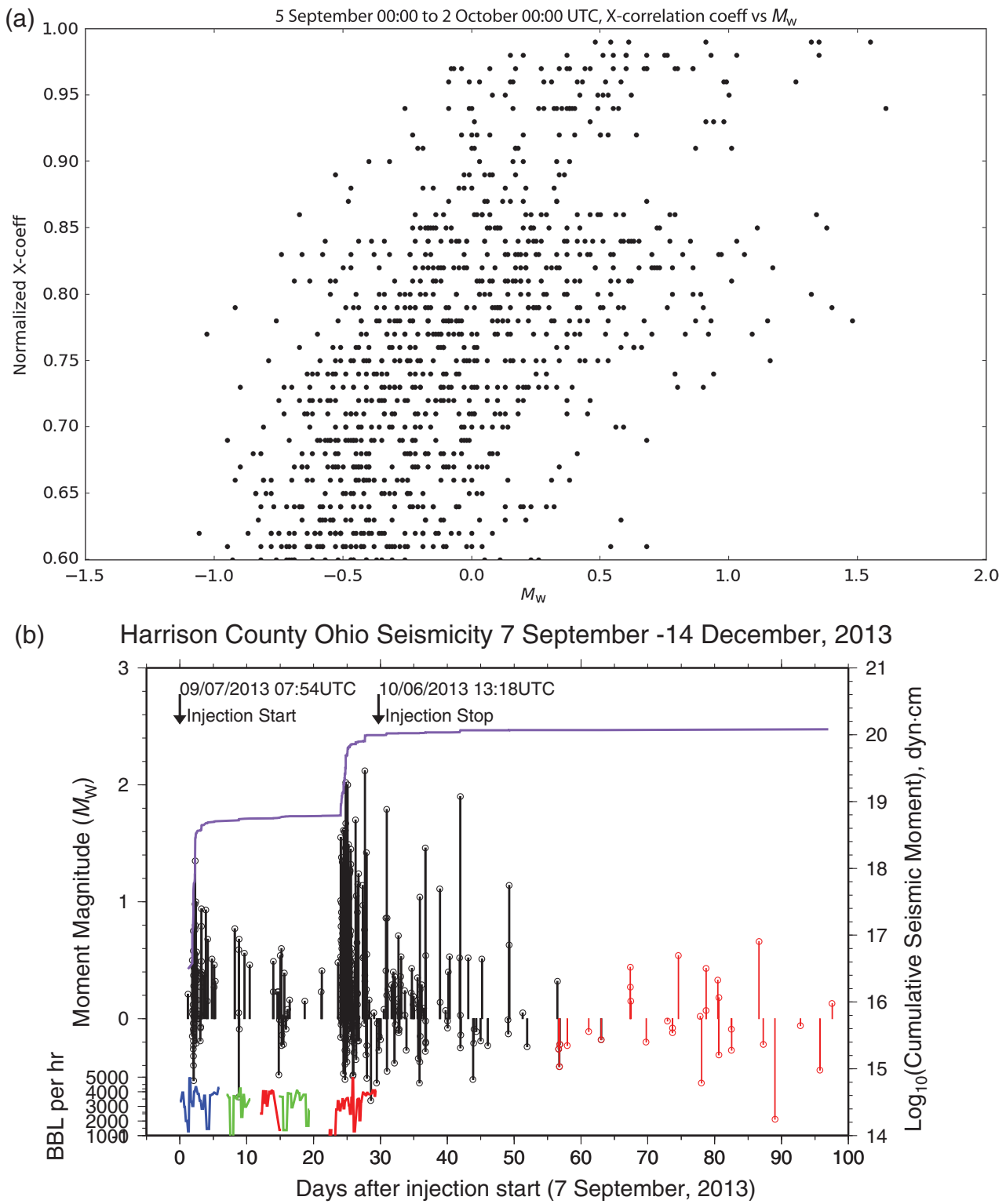
▲ Figure 2. (a) The location of TA stations deployed in Ohio with the TA stations used (red inverted triangles) in locating the 10 earthquakes observed from 2 to 19 October. The small rectangle around O53A is the region expanded in map (b). (b) The TA station O53A (red triangle) and four portable station locations (green triangles). The 10 regional earthquakes located by HYPOINVERSE (numbered blue error ellipses) are also plotted together with their final locations using HypoDD (solid blue circles). The three horizontal wells stimulated during the early and late part of 2013 are also shown marked at the toe of the horizontal section by the labels R3, R2, and R4. The map projection of their paths is shown as red, blue, and green lines, respectively.

Roberts *et al.* (1989). The back azimuths were computed based on 1 s- and 2 s window measurements around the P arrival for each earthquake. The analysis showed that all of the earthquakes were on average at 174° north azimuth $\pm 14^\circ$ from TA O53A (Fig. 2a), which is inconsistent with the majority of the HYPOINVERSE locations that scatter about the TA O53A station. This inconsistency indicates a need for a better modeling of the velocity structure in the region and a need for station corrections.

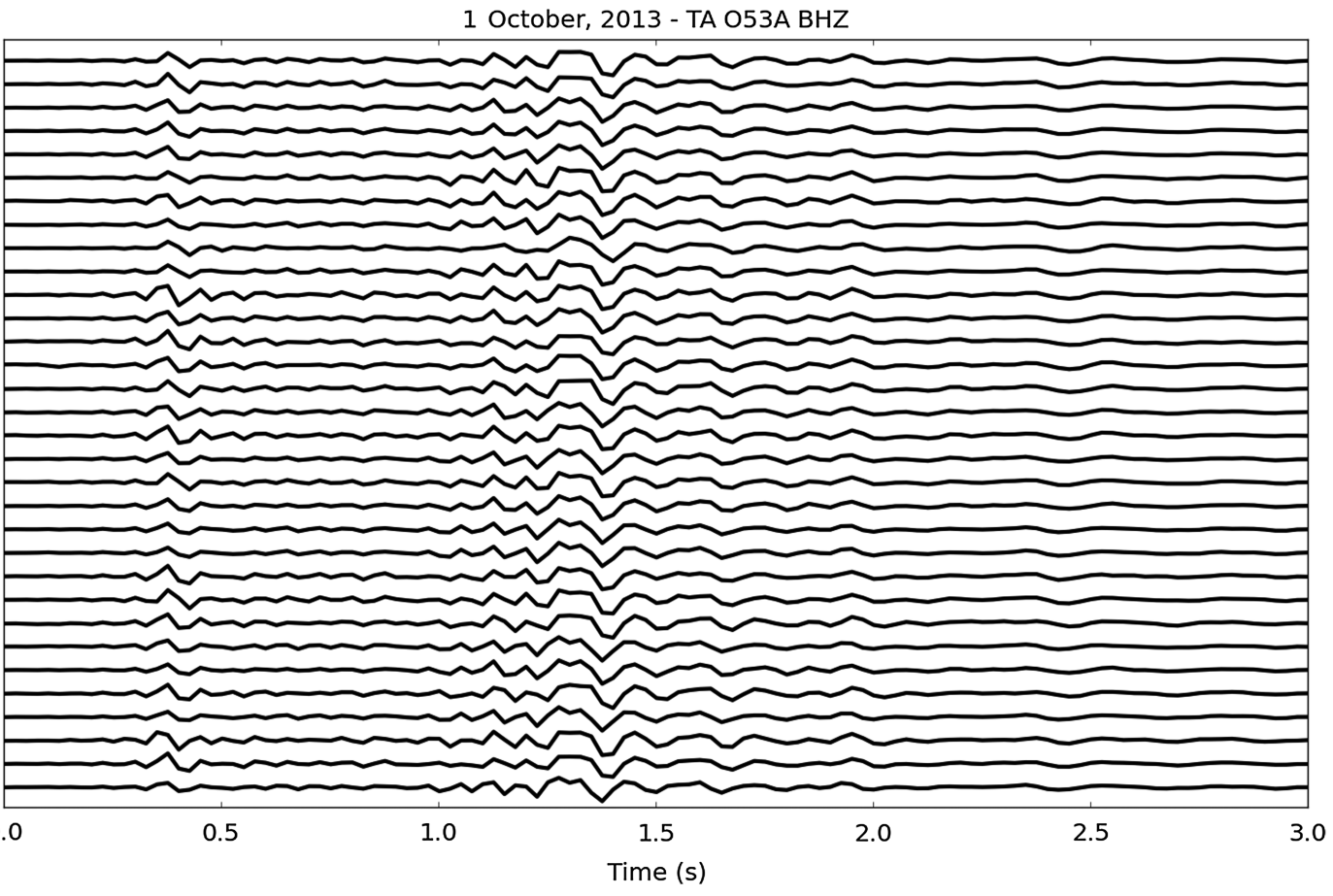
CROSS-CORRELATION TEMPLATE EVENT DETECTIONS

The EarthScope TA stations were primarily deployed to study deep regional structures across the United States continental region. Hence, the next nearest TA stations to O53A are about 50–120 km away. Thus, their records showed poor or no visible signals for small-sized earthquakes located outside the 5 km proximity. Therefore, to determine if there are other possible earthquakes or earthquake sequence in this region prior to the 2 October cluster, the study focused on the O53A station dataset in which we applied a template event cross-correlation signal detection technique (Gibbons and Ringdal, 2006; Holland, 2013; van der Elst *et al.*, 2013; Meng and Peng, 2014) to find lower magnitude earthquakes. The 2 October 10:06 UTC M_w 2.0 earthquake was used as a template event due to its high signal-to-noise ratio (SNR) at the station. The template was built from a 5.0 s window of the vertical component that includes the full waveform: pre- P noise, P arrival, S arrival, and S -coda portion of the earthquake. The event template was filtered from 1.0 to 5.0 Hz and then 10% cosine tapered. Because the template includes the full waveform, matching waveform detections can be assumed to be from earthquakes that are very close to the template event in location and focal mechanisms and therefore are likely to be on the same fault.

The template was applied to over a month of data (1 September to 2 October) prior to the first locatable earthquakes. With a detection threshold ≥ 0.60 for the normalized cross-correlation coefficient, this process produced 1072 earthquake signal detections as shown in Figure 3a. Upon visual inspection, however, we observed that around 15% of the detections were false and some earthquakes with a low SNR were barely resolvable. To improve the event identification, the detection threshold of 0.70 was used, which produced 698 detections with a significant reduction in false detections. In this second set of detected waveforms, however, accurate picks for both P - and S -phase arrivals were still not possible. A detection threshold of 0.85 yielded 298 matches with zero false detections (Fig. 3b), whereas lower thresholds resulted in a progressively greater number of false detections. The earliest among these 298 identified waveforms were observed on 8 September at 06:21 UTC, whereas the greatest density of detections per time interval occurred between 1 October (08:41 UTC) and 2 October (23:59 UTC). During this 39-h period, a total 190 earthquakes were identified whereas the largest number of detections in a single day of 120 occurred on 2 October. Not surprisingly, waveforms



▲ **Figure 3.** (a) Detection cross-correlation coefficients versus M_w magnitude for the TA 053A vertical component from 5 September 2013 00:00 UTC to 2 October 2013 00:00 UTC. (b) Magnitude of the events over time from start of hydraulic fracturing operations on 7 September 2013 (time 0) on Ryser-2, Ryser-3, and Ryser-4 wells with corresponding pumping rates shown in blue, red, and green, respectively. The black lines and circles represent earthquakes with detections only (cross-correlation threshold ≥ 0.85) from TA 053A whereas the red lines and circles represent earthquakes located using the OhioNet four portable stations and TA 053A. The purple line represents the cumulative moment over the same time in dyn·cm. There were no detections above cross-correlation threshold 0.85 going back to December 2012 when the station was installed.



▲ Figure 4. Thirty-two similar waveforms aligned on P arrival of event detection matched by cross-correlation detector for the 24-h period on 1 October 2013 00:00 UTC for TA O53A BHZ. The waveforms shown had cross-correlation coefficients greater than 0.94, with magnitudes in the range from M_w 0.0 to 1.54. All waveforms were band-pass filtered from 1 to 10 Hz and scaled to plot in the same vertical window size showing 3 s of data.

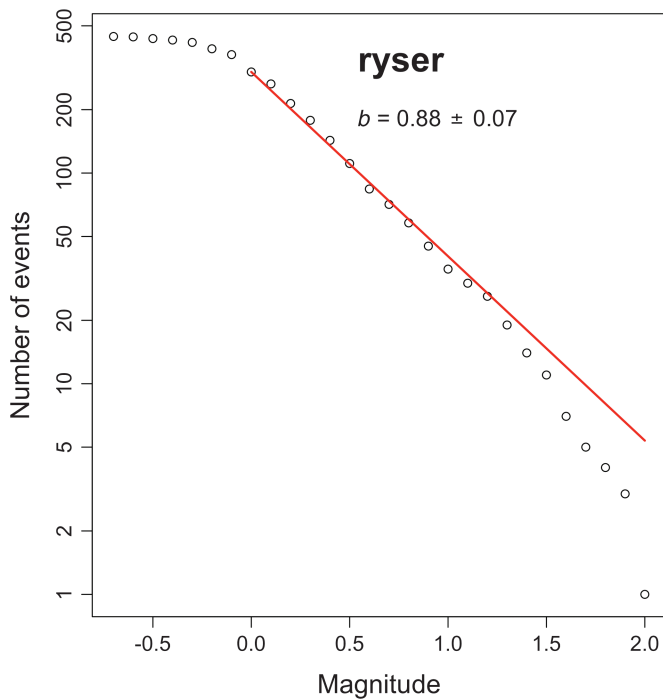
for each of the detections were very similar to the M_w 2.0 event with analogous $S-P$ times and comparable first motions for higher SNR records. Examples of waveforms detected by cross correlation are shown in Figure 4.

To determine whether any earthquakes occurred prior to 7 September, the cross correlation was further applied on the TA O53A data as far back as the station installation date of 13 December 2012 using the same template and the lower coefficient threshold of 0.60. After visually inspecting all detections prior to the start of injection, we observed there were a few false detections but no earthquakes. Results showed no other signals in this area matching the template. In contrast, an additional 180 earthquakes were detected by applying the same cross-correlation event template to the TA O53A data from 3 October through 31 December 2013. The last of these earthquake detections was on 13 December 2013 (22:08 UTC); no further detections were observed after this date. With the assumption that the earthquakes occurred at the same relative location, magnitudes for the detections were established by computing the rms amplitude ratios of a 1.0 s window centered around the P arrival relative to the template (Kim and Chapman, 2005; Kim, 2013). Using a change-point detection

technique (Amorèse, 2007) with the entire population of magnitudes, we calculated a magnitude of completeness of M_w 0.0 and a b -value of 0.88 ± 0.08 as shown in Figure 5.

COINCIDENT HYDRAULIC FRACTURING OPERATION IN THE REGION

Based on the publicly available Ohio Department of Natural Resources (ODNR) map of oil and gas wells in the area, at least seven horizontal wells had undergone hydraulic fracturing from February to October of 2013 near and around Clendenning Lake, particularly the Boy Scout and Ryser wells. Interestingly, the Boy Scout wells located almost beneath O53A station were stimulated in early 2013 but showed no corresponding activity on the seismic record at the TA station. Ryser-2, Ryser-3, and Ryser-4 wells, however, are three horizontal wells that were hydraulically stimulated in the area from early September up to the first week of October 2013. Based on reports submitted to ODNR, these wells were drilled horizontally into the Ordovician age Point Pleasant formation at the depth of ~2422 m from the surface and are parallel to each other trending north-northwest ($\sim 325^\circ$ N azimuth) and extend to approximately 1.5 km (Fig. 1).



▲ **Figure 5.** Gutenberg–Richter magnitude plot with cumulative number of earthquakes greater than a given M_w as circles (0.1 magnitude bin) shown on the vertical axis and M_w magnitude on the horizontal axis. The regression (red line) for b -value is using change-point detection algorithm automatically determining a minimum magnitude of completeness of M_w 0.0 to determine a b -value of 0.88 ± 0.07 .

The total horizontal separation of the three wells was ~370 m between Ryser-3 and Ryser-2 and ~270 m between Ryser-2 and Ryser-4. Hydraulic fracturing of Ryser-2 began on 7 September at 04:36 UTC and continued over 20 stages until 13 September at 02:07 UTC. The second fractured well was the Ryser-4 with 24 stages starting on 14 September at 03:55 UTC and ending on 26 September at 13:03 UTC. The last well fractured with over 47 stages was Ryser-3 from 19 September at 03:57 UTC to 6 October at 13:18 UTC. The volumes of fluid injected into the three wells during the above operations were 24,500 m³ for Ryser-2, 39,500 m³ for Ryser-3, and 30,175 m³ for Ryser-4. Rates of injection for each stage (1000–4000 BBL/hour) and maximum surface pressures were comparable for each well (8000–12,000 pounds per square inch). The operator performed no microseismic monitoring for any of the Ryser wells during the above operations.

Correlation of detected earthquakes with the hydraulic fracturing stages indicates that the first positive magnitude earthquake observed was about 26 h after the stimulation had started. As hydraulic fracturing progressed at each well, there was an apparent increase and tapering off in the rate of event detections per hour as the fracture stimulation began and ended, respectively (Fig. 3b). Moreover, the Ryser-3 stimulation correlated with the most dramatic increase in rate of signal detections, coincident with stages 22 through 31 on 1 to 2 October (Figs. 3b).

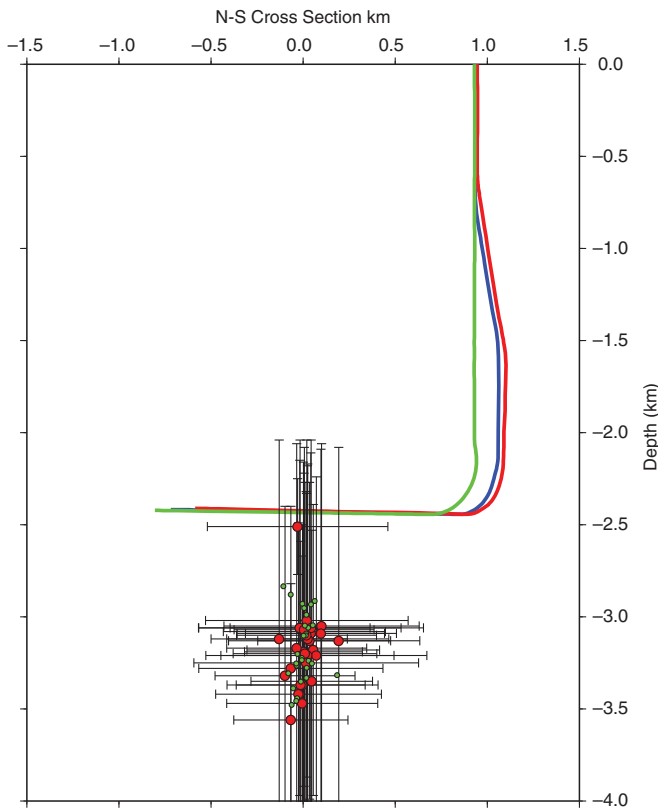
PORTABLE NETWORK DEPLOYMENT AND RESULTS

Because of the location of this earthquake sequence in a region where no seismicity was observed prior, and its proximity to a region with numerous hydraulic fracturing operations, Ohio Department of Natural Resources-Division of Oil and Gas Resources Management deployed in the epicentral area four portable seismic stations with three-component short-period sensors (model L22E; Fig. 2b). Starting from 30 October 2013, data from this network was telemetered over cellular modems near real time with a 200 Hz sampling rate as part of the OhioNet regional seismic network (Besana-Ostman, 2013), which is equipped with an Earthworm seismic processing system (Johnson *et al.*, 1995). Through initial analysis of data from OhioNet's OHH1, OHH2, OHH3, and OHH4 stations, the seismicity associated with the earthquake sequence had decreased and only eight earthquakes were detected and located using HMSC, a proprietary software package. Thus, to increase the usable data from OhioNet stations, the detection cross correlation was reapplied to O53A data with a lowered coefficient threshold of 0.70. In this process, daily results were reviewed manually to remove false detections. From 30 October through 13 December, 30 earthquakes were observed and identified on the TA O53A station that had corresponding records at the four OhioNet stations. The magnitudes of the earthquakes were measured with the same method as the earlier detections, using the rms ratio of the P arrival of the TA O53A vertical component, and ranged from M_w –0.8 to 0.7. P and S arrivals were manually picked. HYPOINVERSE was used to locate all of the earthquakes using the NE Ohio velocity model. Consequently, 27 out of the 30 earthquakes were located using records from all five stations in the network (Table S3). The remaining three earthquakes had only four stations in operation due to a timing problem on OHH1. The earthquake locations had an average rms of 0.013 ± 0.005 s with horizontal uncertainty averaging 400 ± 86 m and vertical uncertainty averaging 868 ± 157 m. All earthquakes were located directly beneath the Ryser wells and define an east–west linear cluster with an average depth of 3.3 km below the surface and a range of depths from 3.0 to 3.6 km.

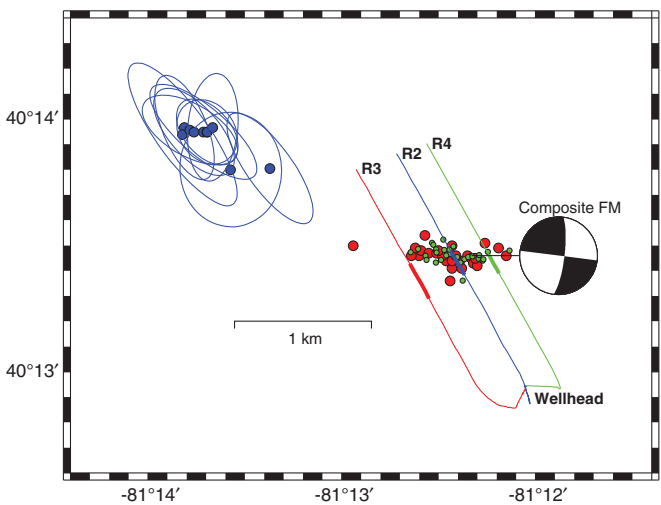
To improve the accuracy of the absolute location of the earthquakes from the portable network, an improved 1D velocity model was needed. To produce such velocity model, a Wadati plot (Wadati, 1933) of the 30 earthquakes' S – P versus P times was fit with a linear regression to determine a V_p/V_s ratio. This resulted in a V_p/V_s ratio of 1.68 in which outliers greater than one standard deviation were filtered out prior to a second linear regression, which produced a V_p/V_s ratio of 1.70. To correct the layer 1 thickness of the NE Ohio velocity model, which is the consolidated Paleozoic sedimentary rocks above the crystalline Precambrian basement, we used the Ohio Precambrian basement contour map from Baranowski (2002) to determine the depth of the crystalline basement in the region (~3.0 km from the surface). With the derived V_p/V_s ratio and the corrected basement depth for NE Ohio velocity model

as a starting point, we performed an inversion for an improved localized 1D velocity model using the VELEST software (Kissling *et al.*, 1994). After three iterations, the inversion arrived at a new model with P -wave velocities of layer 1 and layer 2 of the NE Ohio velocity model that were reduced slightly (0.01 km/s) herein named “Harrison velocity model” (Table S4). Using HYPOINVERSE with the Harrison velocity model, the average rms of the earthquakes improved to 0.011 ± 0.004 s. Four other more complexly layered velocity models were derived based on the available sonic logs on nearby wells to test with formation tops determined from the Ryser wells. However, the use of these other models produced higher location uncertainties and none reduced the overall rms as well as the Harrison 1D model and were therefore all subsequently rejected.

Cross-section and map views of the 30 earthquakes reveal a linear east–west-trending structure at an average depth of 3.2 km from the surface (Figs. 6 and 7). To further constrain the locations of the 30 earthquakes and minimize the uncertainty in the velocity model, we used HypoDD with manual phase picks in an SVD inversion to obtain precise relative locations. Uncertainties from this relative location were 27 m North–South, 10 m east–west, and 44 m in vertical using the Harrison velocity model. Rotating the data in a 3D aspect delineates a planar structure trending N 92° and dipping steeply



▲ Figure 6. North–south cross section perpendicular to strike of preferred fault plane. Red circles represent HYPOINVERSE locations with error bars, and green circles are the same earthquakes relocated with HypoDD.

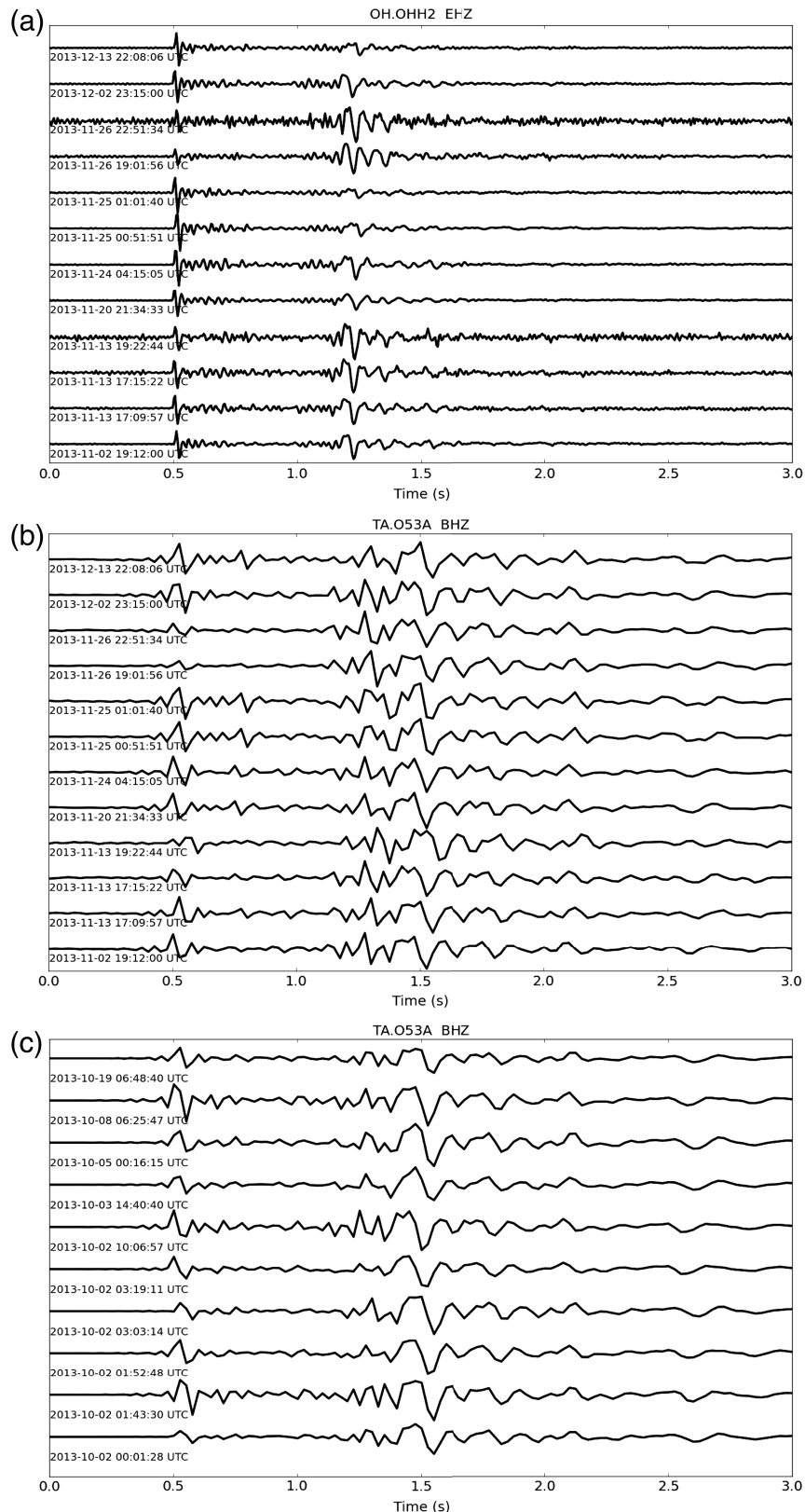


▲ Figure 7. A map view showing the 30 well-located earthquakes with initial HYPOINVERSE locations as red circles and HypoDD locations as green circles. The HypoDD locations of the 10 large earthquakes are shown as blue circles, with error ellipses from the original HYPOINVERSE location. The thickly colored sections of the well paths highlight the hydraulic fracturing stages that correlate with the highest number of detected seismicity. The composite focal mechanism is also plotted for reference.

to the north. The depths of the relocated earthquakes vary between 2.8 and 3.4 km from the surface.

The waveforms from the OhioNet portable network are very similar (Fig. 8a) for different earthquakes, which is indicative of a similar source. The TA O53A waveforms for the 30 well-located earthquakes likewise show high cross-correlation coefficients (ranging from 0.70 to 0.94) with the M_w 2.0 event template (Fig. 8b). Furthermore, S minus P differential travel times for the 30 earthquakes measured at TA O53A are on average 0.68 ± 0.02 s indicating that the well-located earthquakes are slightly further away from TA O53A than the 10 regionally located larger earthquakes.

P -arrival first motions for all of the earthquakes in the sequence were consistent at all stations: compressional at TA O53A, OHH2, and OHH3 and dilatational at OHH1 and OHH4. Because of limited azimuthal coverage of stations around the earthquake source and given the consistency of first motions, we derived a composite focal mechanism with five stations of the portable network using FPFIT method (Reasenberg and Oppenheimer, 1985). The derived composite focal mechanism shows a left-lateral strike-slip mechanism having limited scatter in P and T axes. Along-strike uncertainty is $\pm 10^\circ$, and dip uncertainty is $\pm 11^\circ$ (Fig. 9). The vertical east–west-striking focal plane is close to the structure defined by the earthquake locations and supports the interpretation of a single fault source. It is interesting to note that for other induced earthquake sequences in Ohio, similarly oriented left-lateral strike-slip focal mechanisms have been observed (Seeger *et al.*, 2004; Kim, 2013; Skoumal, 2014). Although the COCORP OH-2 seismic reflection line transects this region, the targets of that study were deeper Grenville basement structure and no near-surface faults



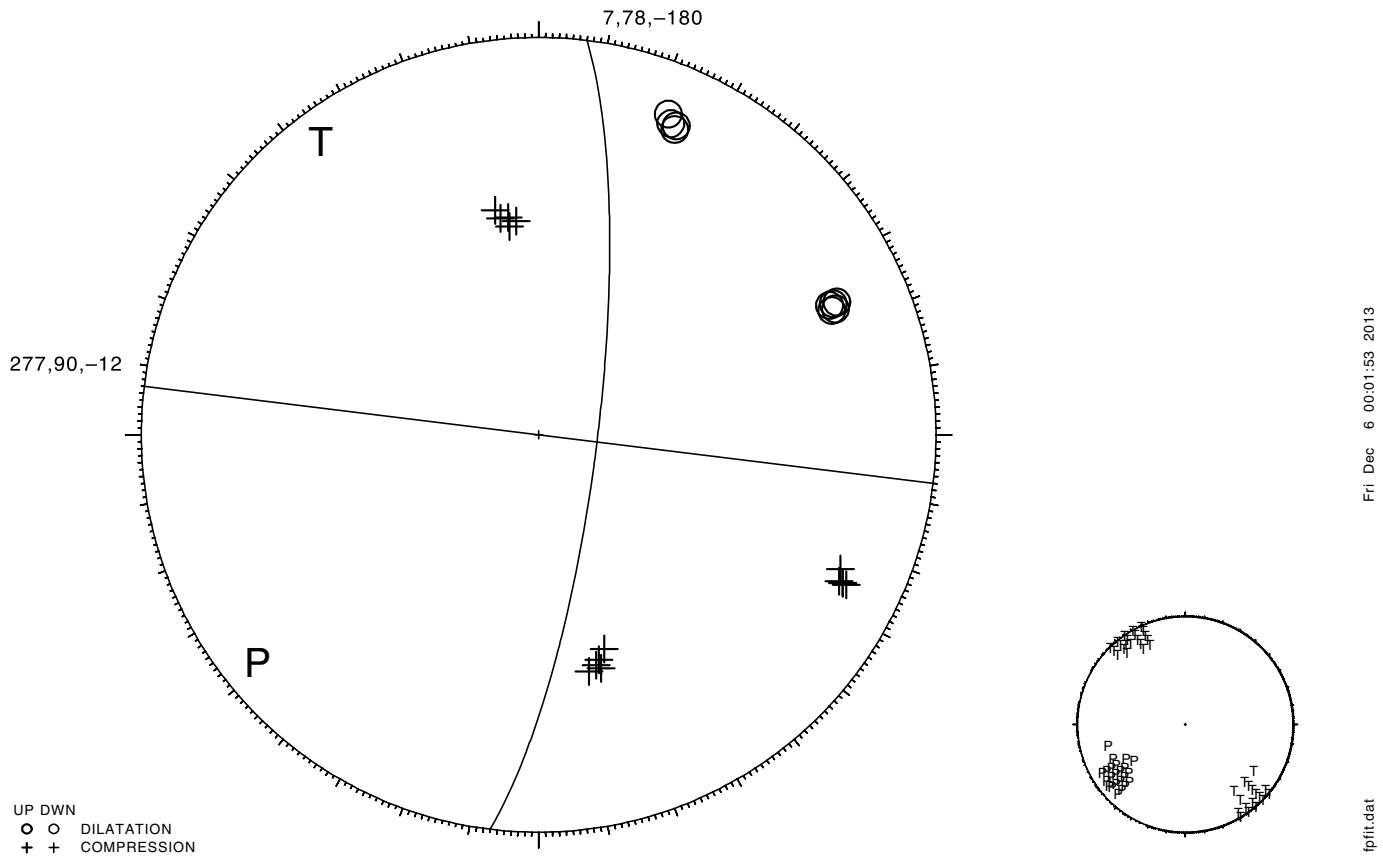
▲ **Figure 8.** A plot showing unfiltered waveforms of the largest 12 well-located aftershocks using the portable network as observed at (a) station OHH2 on the vertical EH.Z component and (b) on the TA 053A station vertical BH.Z component band-pass filtered from 1 to 20 Hz to remove long-period signals. The character of the TA 053A waveforms is very similar with high correlation coefficients (0.73–0.97) to the larger earthquakes located only using the TA network. The unfiltered TA 053A BH.Z component (from Fig. 1a) is shown again for comparison in (c).

20131125 19:01 56.52
 40 13.46 81 12.33
 DEPTH = 3.10 KM
 MAG = 0.00

RMS = 0.01 S
 DMIN = 3 KM
 AZM GAP = 193
 # FM = 24

ERH = 0.3 KM
 ERZ = 0.8 KM
 MISFIT = 0.00 (+.03)
 STDR = 0.66

STRIKE UNCERTAINTY = 10
 DIP UNCERTAINTY = 11
 RAKE UNCERTAINTY = 20
 % MACHINE PICKS = 0



▲ **Figure 9.** Composite lower hemisphere first-motion focal mechanism using five earthquakes.

are well resolved in the data ([Culotta et al., 1990](#)). Furthermore, the COCORP OH-2 line ran parallel to the strike of the inferred fault, which would not have helped in resolving it. Unfortunately, there are no publicly available seismic-reflection profiles through the region and no basement fault mapped by the Ohio Geological Survey.

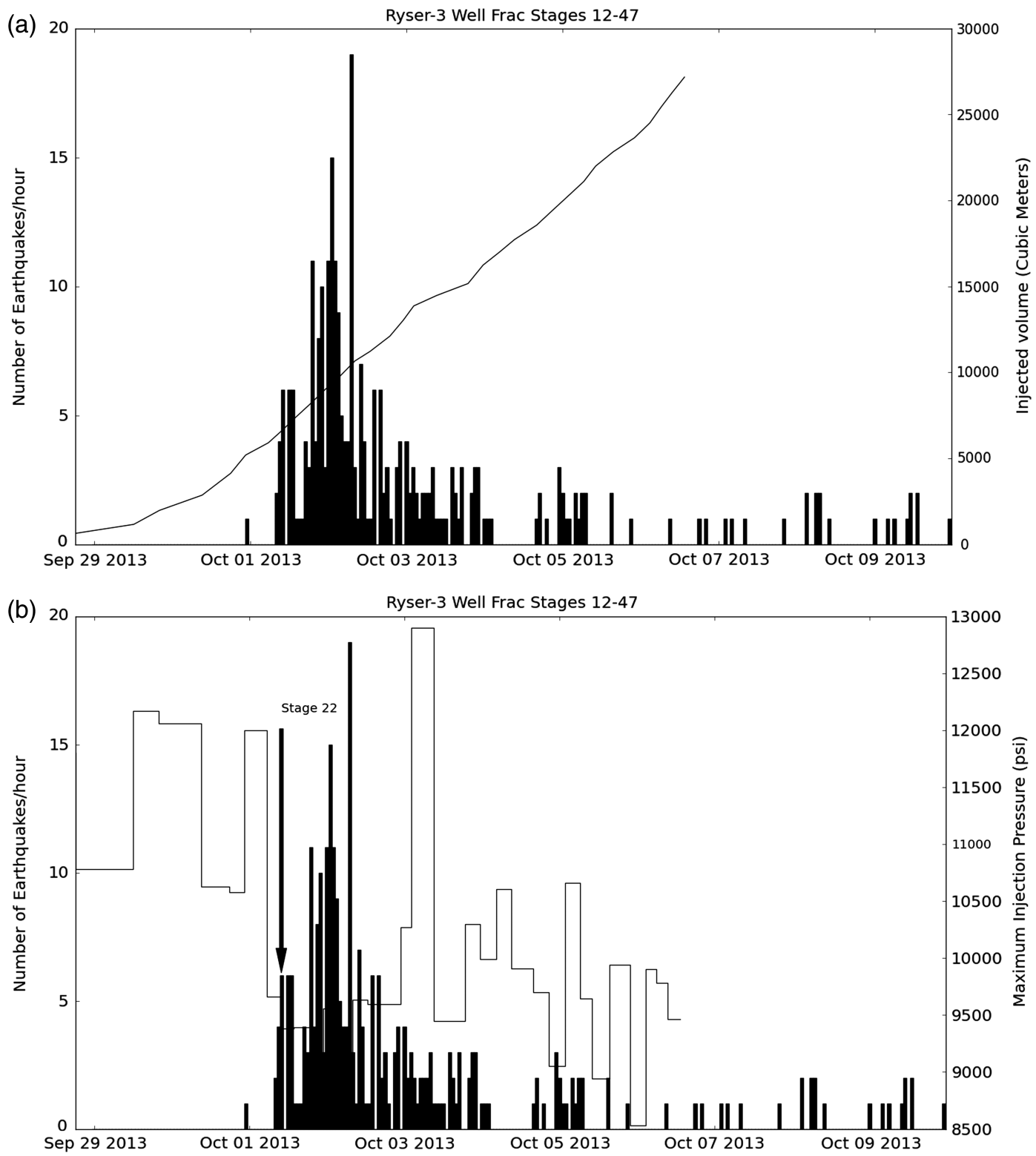
DISCUSSION

Locations using an NE Ohio velocity model of the Harrison earthquake sequence, which occurred from 2 to 19 October, were estimated to be about 800–1500 m west of the three Ryser wells. The depths of these events are 1.4 ± 1.0 km below the horizontal levels of the wells or about 3.8 ± 1.0 km from the surface. These depths place the earthquakes in the crystalline Precambrian basement. However, back-azimuth analysis of the three-component data of the closest TA station indicates that the source of the P arrival is on average N174° azimuth, which point directly to the location of the Ryser wells. Thus, the absolute location of the earthquakes using a regional velocity model (Fig. 2) is inconsistent with the azimuthal analysis. This discrepancy is most probably due to the geometry of the

stations used in the calculations, using only a 1D regional velocity model, the absence of station corrections, and use of a least-squares location algorithm.

However, despite the location inconsistency and uncertainty, the earthquakes temporal occurrence identified through template matching more or less coincides with the hydraulic fracturing operations. Moreover, the double-difference locations using cross correlation of phases show a tight linear clustering of the earthquakes, which is consistent with the similarity of waveforms for each earthquake. The obvious scatter in the initial locations observed in Figure 2b can therefore be explained by the uncertainty on manual picks combined with the use of a regional velocity model and no station corrections.

On the other hand, waveform signals from seismic events induced by hydraulic fracturing have been known to have a high degree of similarity as observed by surface monitoring ([Eisner et al., 2008; Hulsey et al., 2009](#)) and through downhole monitoring ([Rutledge and Phillips, 2003](#)). Waveform similarity has been noted for the sets of data through cross-correlation master event template technique: one that used mainly the TA O53A station at the beginning of the earthquake sequence and another one that utilized the OhioNet array. Thus, the



▲ **Figure 10.** Seismic activity for the time Ryser-3 stages 12–47 were fractured, versus (a) cumulative injection volume in cubic meters and (b) maximum injection pressures (psi) measured at the surface.

similarity of waveforms (refer to Figs. 1, 4, and 8) noted in this study most probably indicates that the Harrison earthquake sequence originated in the same source location area despite the discrepancy in their initial locations.

In terms of timing, the observed earthquake sequence began within 26 h after the start of hydraulic fracturing operations at Ryser-2. The earthquake count also increased progressively through time as the fracture operations continued.

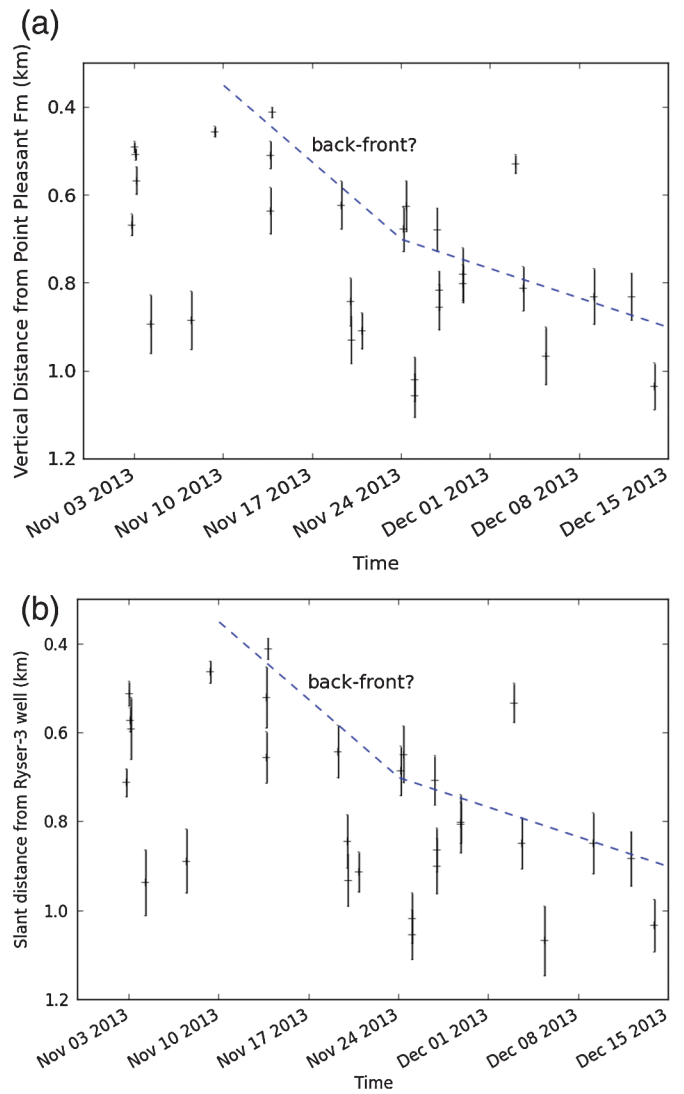
Interestingly, the maximum count in detections on 2 October is coincident in time with fracture operations on the Ryser-3 well wherein the maximum injection pressure was highest during the stimulation. The earthquake activity increased during hydraulic fracturing at stages 22–25 of Ryser-3 (Fig. 10). Stages located at the same vicinity in both Ryser-2 and Ryser-4 were also correlated with increased detections (Fig. 7). Such precise time–space correlation indicates strong coupling between the pulse of increased formation pore pressure and the seismogenic fault approximately 0.6 km directly below in the basement.

The well-located 30 earthquakes situated immediately beneath the horizontal wells clearly delineate a linear east–west-trending structure beneath the Ryser-2, Ryser-3, and Ryser-4. Results of the composite focal mechanism determination likewise indicate an east–west-trending strike-slip fault for these events. The earthquakes distribution defines a plane at least \sim 500 m long-trending east–west that extends from 3.0 to 3.5 km depth below the surface. This extent of the fault clearly indicates that the fault rupture activity produced during the operation occurred below the formation where the fracturing is supposed to remain confined to. Typical injection-related seismicity has b -values closer to 2.0 (Maxwell *et al.*, 2009) for populations of new fractures being generated and b -values closer to 1.0 for opening of pre-existing fractures. The b -value of all the detected events is close to 1.0. This b -value suggests activation of a pre-existing fault rather than the creation of new fractures as intended by the injection operations.

Correlation between seismic activity and maximum injection pressure or injected fluid volume for Ryser-3 stages 21–47 show no apparent relationship due to the comparable injection pressures and volumes for each stage of all of the Ryser wells (Fig. 10). However, it can be surmised that the Ryser-3 had a better hydraulic linkage with the pre-existing fault compared to the other two wells, which were located further eastward. Hence, stimulation operations in the two eastern wells had lower numbers of events. Figure 11 shows a pattern of the 30 aftershock earthquakes mostly occurring deeper and farther from the Ryser-3 with time, indicating a possible back-front of the seismic activity (Parotidis *et al.*, 2004). Such a temporal trend can be an indication of pore-pressure diffusion through time. Overall, the absence of seismicity in the area prior to 8 September, the peak of activity during particular stages along the wells, and the gradual tapering off of seismicity as the injection and flowback operations ceased are very much indicative of a close relationship to overall Ryser wells operations.

On the other hand, hydraulic operations occurred directly beneath the TA 053A station in May 2013 along Boy Scout 4, 5, and 6 wells. There was no clear observable earthquake signal at the station during these operations. This implies that microseismicity produced during such operations did not reach positive magnitudes and consequently stayed below the detection threshold of a TA station.

Davis and Frohlich (1993) developed three primary criteria to determine if seismicity is induced by fluid injection activities: (1) coincident timing, (2) coincident location, and (3) adequate fluid pressures. In the case of Harrison sequence,



▲ Figure 11. (a) Vertical distance of the 30 postinjection earthquakes from the target hydraulic fracture formation versus time. (b) The slant distance from a point on the Ryser-3 well bore where the east–west seismicity pattern projects vertically into it. The dashed line, drawn free-hand in plot (a) shows a possible back-front of seismicity.

the first two criteria were positively achieved and thus indicative of induced seismicity due to hydraulic fracture stimulation. Despite the absence of fault encountered during the drilling logs (personal communication with operator), adequate pressures would have been introduced to cause positive magnitude earthquakes along a pre-existing unknown structure that was in a state of near failure. Because the ultimate goal of any hydraulic fracturing operation is to stimulate crack growth, earthquakes are expected as a consequence. However, positive magnitude earthquakes triggered during such operations are still rare and uncommon. To produce and stimulate cracks beyond the target formation is undesirable both for purposes of good production and for safety, especially if cracks were to propagate into a shallower formation above the target formation. In the

case of the Harrison earthquake sequence, the induced seismicity indicated faulting below the target formation.

CONCLUSIONS

The portable network data with double-difference location of earthquakes clearly show a vertical east–west-trending fault directly beneath the Ryser-2, Ryser-3, and Ryser-4 horizontal wells. The fault is located in the Precambrian crystalline basement formation and not in the Paleozoic formations in which the wells were located. Further, the highest concentration of cross-correlation detections along the well bores aligns with the portable earthquake locations, indicating that a possible hydraulic pathway to the basement fault exists through the Paleozoic formations. The 10 widely observed positive magnitude earthquakes located in the October 2013 Harrison County, Ohio, earthquake sequence are spatially and temporally linked with the hydraulic fracture operations at the nearby Ryser wells through similarity of waveforms with the portable network. Other numerous seismic events detected from cross correlation show that the start and tapering off of seismic activity is coincident with start and culmination of hydraulic operations, respectively, with some temporal delay. The remarkable similarity of waveforms between all of the earthquakes detected during the hydraulic fracturing operations and afterward indicates a common source. Based on all of these corroborating pieces of evidence, it is most probable that hydraulic fracturing on the Ryser wells induced the 2013 Harrison earthquake sequence. ■

ACKNOWLEDGMENTS

Funding for this research came from Instrumental Software Technologies, Inc. and station deployments from Ohio Department of Natural Resources-Division of Oil and Gas Resources Management (ODNR-DOGRM). This paper benefited from discussions with Austin Holland of the Oklahoma Geological Survey and Leonardo Seeber of Lamont–Doherty. The Transportable Array data used were from Incorporated Research Institutions for Seismology EarthScope project (www.iris.edu, last accessed September 2014) and portable stations from ODNR-GeoSurvey. Our further thanks go to Felix Waldhauser for tips and assistance with HypoDD, Austin Holland for contributing his ObsPy routines, and Won-Young Kim for his Generic Mapping Tools (GMT) script used in the detection over time plot (Fig. 3). ObsPy (Beyreuther *et al.*, 2010) with matplotlib was used for the cross-correlation technique and related figures and GMT (Wessel and Smith, 1991) was used for some of the figures. Well location and completion reports were provided by Gulfport Energy to ODNR-DOGRM as part of compliance and are accessible on the web as of 2014. We wish to thank the *SRL* editor and an anonymous reviewer for suggestions that helped to improve the paper.

REFERENCES

- Amorèse, D. (2007). Applying a change-point detection method on frequency–magnitude distributions, *Bull. Seismol. Soc. Am.* **97**, 1742–1749, doi: [10.1785/0120060181](https://doi.org/10.1785/0120060181).
- Baranoski, M. T. (2002). Structure contour map on the Precambrian unconformity surface in Ohio and related basement features, *ODNR Report Map PG-23*, scale 1:500,000, 27 pp.
- Besana-Ostman, G. M. (2013). Earthquake seismic risk reduction in Ohio: ODNR's efforts to address issues with natural and induced seismicity, in *AGU Meeting of the Americas Abstracts*, Cancun, Mexico, May 2013.
- Beyreuther, M., R. Barsch, L. Kischer, T. Megies, Y. Behr, and J. Wasser mann (2010). ObsPy: A Python toolbox for seismology, *Seismol. Res. Lett.* **81**, no. 3, 530–533.
- British Columbia Oil and Gas Commission (BCOGC) (2012). Investigation of observed Seismicity in the Horn River Basin, *British Columbia Oil and Gas Commission Report*, 29 pp.
- Culotta, R. C., T. Pratt, and J. Oliver (1990). A tale of two sutures: CO-CORPS's deep seismic surveys of the Greenville province in the eastern midcontinent, *Geology* **18**, 646–649.
- Davis, S. D., and C. Frohlich (1993). Did (or will) fluid injection cause earthquakes?—Criteria for a rational assessment, *Seismol. Res. Lett.* **64**, nos. 3/4, 207–224.
- de Pater, C. J., and S. Baisch (2011). Geomechanical study of Bowland Shale seismicity: Synthesis report, Report 71, Department of Energy and Climate Change.
- Eisner, L., D. Abbott, W. B. Barker, J. Lakings, and M. P. Thornton (2008). Noise suppression for detection and location of microseismic events using a matched filter, *SEG Expanded Abstracts* **27**, 1431.
- Gibbons, S. J., and F. Ringdal (2006). The detection of low-magnitude seismic events using array-based waveform correlation, *Geophys. J. Int.* **165**, 149–166.
- Hansen, M., and L. J. Ruff (2003). The Ohio seismic network, *Seismol. Res. Lett.* **74**, no. 5, 561–564.
- Havskov, J., and L. Ottemöller (1999). SeisAn Earthquake analysis software, *Seismol. Res. Lett.* **70**, http://www.seismosoc.org/publications/SRL/SRL_70/srl_70-5_es.html (last accessed September 2014).
- Holland, A. (2011). Examination of possibly induced seismicity from hydraulic fracturing in the Eola field, Garvin County, Oklahoma, *Oklahoma Geol. Surv. Open-File Rept. OFI-2011*, 28 pp.
- Holland, A. (2013). Earthquakes triggered by hydraulic fracturing in south-central Oklahoma, *Bull. Seismol. Soc. Am.* **103**, no. 3, 1784–1792, doi: [10.1785/0120120109](https://doi.org/10.1785/0120120109).
- Hulsey, B. J., L. Eisner, M. P. Thornton, and D. Jurick (2009). Application of relative location technique from surface arrays to microseismicity induced by shale fracturing, *SEG Expanded Abstracts* **28**, 1602.
- Johnson, C. E., A. Bittenbinder, B. Bogaert, L. Dietz, and W. Kohler (1995). Earthworm: A flexible approach to seismic network processing, *Incorporated Research Institutions for Seismology (IRIS) Newsletter* Vol. 14, 1–4.
- Kim, W. Y. (2013). Induced seismicity associated with a fluid injection into deep well in Youngstown, Ohio, *J. Geophys. Res.* **118**, 3506–3518, doi: [10.1002/jgrb.50247](https://doi.org/10.1002/jgrb.50247).
- Kim, W. Y., and M. Chapman (2005). The 9 December 2003 central Virginia earthquake sequence: A compound earthquake in the central Virginia seismic zone, *Bull. Seismol. Soc. Am.* **95**, 2428–2445.
- Kissling, E., W. L. Ellsworth, D. Eberhart-Phillips, and U. Kradolfer (1994). Initial reference model in local earthquake tomography, *J. Geophys. Res.* **99**, 19,635–19,646.
- Klein, F. W. (2007). User's guide to HYPOINVERSE-2000, a Fortran program to solve for earthquake locations and magnitudes, *U.S. Geol. Surv. Open-File Rept. 02-171*, 121 pp.
- Lienert, B. R. E., and J. Havskov (1995). A computer program for locating earthquakes both locally and globally, *Seismol. Res. Lett.* **66**, 26–36.
- Lienert, B. R. E., E. Berg, and L. N. Frazer (1986). Hypocenter: An earthquake location method using centered, scaled, and adaptively least squares, *Bull. Seismol. Soc. Am.* **76**, 771–783.

- Maxwell, S. C., M. Jones, R. Parker, S. Miong, S. Leany, D. Dorval, D. D'Amico, J. Logel, E. Anderson, and K. Mammermaster (2009). Fault activation during hydraulic fracturing, *2009 SEG Annual Meeting*, 25–30 October 2009, Houston, Texas, 5 pp.
- Maxwell, S. C., T. I. Urbancic, N. Seinsberger, and R. Zinno (2002). Microseismic imaging of hydraulic fracture complexity in the Barnett Shale, *SPE Annual Technical Conference and Exhibition*, 29 September–2 October 2002, SPE 77440, 9 pp.
- Meng, X., and Z. Peng (2014). Seismicity rate changes in the San Jacinto Fault Zone and the Salton Sea geothermal field following the 2010 M_w 7.2 El Mayor-Cucapah earthquake, *Geophys. J. Int.* **197**, no. 3, 1750–1762, doi: [10.1093/gji/ggu085](https://doi.org/10.1093/gji/ggu085).
- Ottemöller, L., and J. Havskov (2003). Moment magnitude determination for local and regional earthquakes based on source spectra, *Bull. Seismol. Soc. Am.* **93**, 203–214.
- Parotidis, M., S. A. Shapiro, and E. Rothert (2004). Back front of seismicity induced after termination of borehole fluid injection, *Geophys. Res. Lett.* **31**, 885–887.
- Reasenberg, P., and D. Oppenheimer (1985). Fpfit, fpplot, and fppage: Fortran computer programs for calculating and displaying earthquake fault plane solutions, *Technical Report, U.S. Geol. Surv. Open-File Rept.* 85-793.
- Roberts, R. G., A. Christoffersson, and F. Cassidy (1989). Real time events detection, phase identification and source location estimation using single station component seismic data and a small PC, *Geophys. J. Int.* **97**, 471–480.
- Rutledge, J. T., and W. S. Phillips (2003). Hydraulic stimulation of natural fractures as revealed by induced microearthquakes, Carthage Cotton Valley gas field, east Texas, *Geophysics* **68**, no. 2, 441–452.
- Schaff, D. P. (2008). Semiempirical statistics of correlation-detector performance, *Bull. Seismol. Soc. Am.* **98**, 1495–1507.
- Schaff, D. P., and F. Waldhauser (2010). One magnitude unit reduction in detection threshold by cross correlation applied to Parkfield (California) and China seismicity, *Bull. Seismol. Soc. Am.* **100**, 3224–3238, doi: [10.1785/0120100042](https://doi.org/10.1785/0120100042).
- Seeber, L., J. Armbruster, and W. Y. Kim (2004). A fluid-injection-triggered earthquake sequence in Ashtabula, Ohio: Implications for seismogenesis in stable continental regions, *Bull. Seismol. Soc. Am.* **94**, 76–87.
- Skoumal, R. J., M. R. Brudzinski, and B. S. Currie (2014). Induced earthquakes during hydraulic fracturing in Poland Township, Ohio, *Bull. Seismol. Soc. Am.* (submitted).
- Stover, C. W., and J. L. Coffman (1993). Seismicity of the United States, 1568–1989 (revised), *U.S. Geol. Surv. Profess. Pap.* 1527, 418 pp.
- van der Elst, Nicholas J., Heather M. Savage, Kathleen Keranen, and Geoffrey A. Abers (2013). Enhanced remote earthquake triggering at fluid-injection sites in the midwestern United States, *Science* **341**, no. 6142, 164–167.
- Wadati, K. (1933). On the travel time of earthquake waves. Part II, *Geophys. Mag. (Tokyo)* **7**, 101–111.
- Waldhauser, F. (2001). hypoDD—A program to compute double-difference hypocenter locations, *U.S. Geol. Surv. Open-File Rept.* 01-113, 25 pp.
- Waldhauser, F., and W. L. Ellsworth (2000). A double-difference earthquake location algorithm: Method and application to the northern Hayward fault, *Bull. Seismol. Soc. Am.* **90**, 1353–1368.
- Wessel, P., and W. H. F. Smith (1991). Free software helps map and display data, *Eos Trans. AGU* **72**, 441, 445–446.

*Paul A. Friberg
Ilya Dricker*

Instrumental Software Technologies, Inc. (ISTI)

New Paltz, New York 12561 U.S.A.

p.friberg@isti.com

*Glenda M. Besana-Ostman¹
Ohio Department of Natural Resources (ODNR)
Division of Oil and Gas Resources Management (DOGRM)
2045 Morse Road
Columbus, Ohio 43229-6693 U.S.A.*

¹ Now at Geophysics and Seismotectonics Group, Technical Service Center, Bureau of Reclamation, Department of Interior, Denver Federal Center, 6th and Kipling Street, Building 67, 10th Floor, Denver, Colorado 80225 U.S.A.